ENGINOM | Engineering Innovations

Available online at www.enginom.org
ENGINOM in Engineering Innovations
(E-ISSN: xxxx-xxxx; ISSN: xxxx-xxxx)
Vol. 1, No. 01, March, 2026

Investigating the shear flexural behavior of NSM FRP-strengthened RC beams by experimentation and numerical analysis

Article,

Abd Al-Kader A. Al Sayed [1,*], A. Ali [2], Mohammed Yahya M. Al-Fasih [1]

1 Department of Civil Engineering, College of Engineering and Information Technology, Onaizah Colleges, Qassim, Saudi Arabia;
2 Department of Civil Engineering, Higher Technological Institute, 10th of Ramadan City 44629, Egypt; Ahmed.ali@hti.edu.eg,
* **Corresponding author**: Abd Al-Kader A. Al Sayed,

Academic Editor:
Essam Mohammed

Submission: 9 May 2026
Revision: 15 May 2026
Acceptance: 13 June 2026

Citation: To be added by editorial staff during production.

Abstract

In recent years, near-surface-mounted (NSM) FRP has become a strong alternative to the externally bonded (EB) technique. Compared to the EB approach, the NSM technology is less susceptible to external damage sources and improves the bond between the FRP reinforcement and the surrounding concrete. However, one of the most common reasons why RC beams reinforced with NSM technology fail is debonding via concrete cover separation (CCS), which begins and ends at low strain levels in the NSM reinforcement. Scientists therefore put a lot of effort into figuring out how to delay or prevent this kind of failure. In this investigation, two different bar configurations with straight and bent ends were used. The purpose of the bent end is to delay or prevent the CCS failure. A numerical analysis utilizing non-linear finite element modeling (FEM) was performed in ANSYS® to confirm the experimental results. Overall, there was good agreement between the numerical results and the corresponding experimental data at each loading level.

Keywords: Strengthening, NSM, CFRP, Debonding, Concrete cover separation, End Anchorage, Finite element modeling, Fracture energy

1. Introduction

In recent years, the application of near-surface-mounted (NSM) fiber-reinforced polymer (FRP) reinforcement has gained widespread recognition as a highly effective technique for strengthening reinforced concrete (RC) structures [1], [2]. The NSM method involves cutting longitudinal slits or grooves into the concrete cover on the tension side of the structural member to be strengthened [3], [4], [5]. These prepared grooves are then filled with an epoxy adhesive, into which FRP bars, strips, or laminates are embedded [6], [7]. This configuration ensures a more integrated and efficient load transfer between the FRP reinforcement and the surrounding concrete [8], [9].

Compared with the conventional externally bonded (EB) FRP technique, the NSM approach offers several distinct advantages, including a significantly improved bond performance due to the larger contact surface and the surrounding concrete confinement, reduced installation time, the ability to anchor the FRP reinforcement directly into adjacent structural members, and inherent protection of the FRP from mechanical damage, fire, and vandalism because it is embedded within the concrete cover rather than exposed on the surface [10], [11]. Despite these superior bond characteristics, however, the possibility of debonding failures is not entirely eliminated [12], [13]. Such failures typically manifest in two primary forms: intermediate crack-induced debonding (ICID), which initiates from a flexural or flexural-shear crack and propagates along the FRP-concrete interface, and concrete cover separation (CCS), which occurs along a failure plane located approximately at the level of the

internal tension steel reinforcement [14], [15]. Among these two failure modes, CCS is considerably more common and often governs the ultimate behavior of NSM FRP-strengthened beams [16], [17].

To control and delay the occurrence of CCS, various anchoring solutions have been proposed and investigated in the literature. Among these, CFRP U-wraps have been utilized as an external transverse anchoring system [18], [19], [20]. Experimental evidence has shown that such transverse anchoring is highly effective in enhancing the ultimate flexural capacity of RC beams strengthened with NSM FRP. This improvement is achieved either by postponing the onset and propagation of CCS [21] or by altering the failure mode entirely, shifting it from a sudden debonding failure to a more ductile failure such as concrete crushing in compression or rupture of the CFRP wrap [22], [23]. In a series of comprehensive studies, Sharaky et al. [2], [11], [24] investigated the bond and flexural behavior of RC beams strengthened with NSM FRP reinforcements. Their experimental program considered multiple critical parameters, including different FRP material types (such as carbon, glass, and basalt), variations in epoxy adhesive properties, different sizes and diameters of NSM bars, and varying numbers of NSM bars per groove [8], [25]. To further delay the onset of CCS, mechanical end anchors were developed and applied. This mechanical anchoring system was created by drilling vertical holes into the concrete, each with a diameter of 10 mm and a depth of 200 mm, into which steel bars were inserted. These steel bars were subsequently connected to a specially designed assembly consisting of a steel plate with a steel tube welded to it. The FRP reinforcement was then anchored to the concrete by bonding its end inside the steel tube. The experimental results obtained from this system demonstrated that mechanical end anchoring successfully postponed the occurrence of CCS and simultaneously improved the structural performance of the tested beams, as evidenced by increased stiffness, higher yield load, and greater ultimate load-carrying capacity compared to beams without such anchoring.

In addition to the extensive body of experimental work reported in the literature, many researchers have also employed three-dimensional finite element (3D-FE) numerical analyses to evaluate the influence of various parameters on the behavior of NSM FRP-strengthened RC beams [8-14]. These parameters include FRP type and reinforcement ratio, groove dimensions, adhesive properties, concrete strength, and bond length, among others. However, it has been widely recognized that the simplified assumption of perfect bonding—i.e., assuming no slip and no gap at the bar-epoxy and epoxy-concrete interfaces—is inherently incapable of accurately predicting FRP debonding failure. In fact, such an idealization significantly overestimates both the ultimate load and the corresponding deflection at failure [8, 9, 14]. Therefore, it is essential to explicitly incorporate the debonding behavior into the finite element modeling (FEM) of NSM FRP-strengthened beams in order to develop accurate simulations that can reliably capture the actual structural response, including the onset and propagation of debonding, the load-deflection curve, and the final failure mode.

In the present research, the authors proposed and investigated a novel bar configuration featuring 90° bent ends as a means to delay CCS failure in RC beams strengthened with NSM FRP. Additionally, the effect of varying the FRP cross-sectional area on the structural behavior of the strengthened beams was systematically examined. Beyond the experimental investigation, a comprehensive numerical study was also carried out using the ANSYS® finite element analysis program. The developed FE models were carefully calibrated and validated against the experimental results. Importantly, these models incorporated the bond behavior specifically at the epoxy-concrete interface, thereby allowing realistic simulation of debonding mechanisms. A detailed comparison between the numerical predictions and the experimental measurements was conducted in terms of the full load-deflection response, including initial stiffness, cracking load, yield behavior, post-yield response, and ultimate load, as well as the

observed failure modes. This comparison served to validate the accuracy and reliability of the proposed FE modeling approach.

1.1. Research Significance

The strengthening of reinforced concrete (RC) structures using near-surface-mounted (NSM) fiber-reinforced polymer (FRP) reinforcement has gained considerable attention as a reliable and efficient retrofitting technique. While extensive research has been conducted on the flexural strengthening of RC beams using NSM FRP systems, the shear flexural behavior—particularly the interaction between flexural and shear mechanisms under combined loading conditions—remains insufficiently explored. Most existing studies have focused either on pure flexure or on separate shear strengthening configurations, with limited attention given to the coupled shear-flexural response that more accurately represents real-world loading scenarios in existing structures.

Moreover, the debonding failure modes associated with NSM FRP-strengthened beams, especially concrete cover separation (CCS) and intermediate crack-induced debonding (ICID), continue to pose significant challenges to the widespread adoption of this technique. Although various anchoring solutions, such as CFRP U-wraps and mechanical end anchors, have been proposed to delay such failures, these methods often add complexity, cost, and installation difficulties. Furthermore, the effectiveness of these anchoring systems under combined shear and flexural demands has not been systematically quantified. In particular, the use of novel bar configurations—such as FRP bars with 90° bent ends—as a means to control CCS while simultaneously enhancing shear-flexural performance has received very little attention in the literature.

On the numerical front, many existing finite element (FE) models of NSM FRP-strengthened beams rely on the oversimplified assumption of perfect bonding at the bar-epoxy and epoxy-concrete interfaces. This assumption fails to accurately predict debonding failures, leading to significant overestimations of load-carrying capacity and deflection. Consequently, there is a critical need for validated FE models that explicitly incorporate interface bond behavior to reliably simulate the onset and propagation of debonding under combined shear and flexural loading.

Therefore, the significance of this research stems from its dual experimental and numerical investigation into the shear-flexural behavior of RC beams strengthened with NSM FRP systems. The study introduces a novel NSM bar configuration with 90° bent ends as a practical and efficient anchoring solution to delay CCS failure. In parallel, the research develops and validates advanced three-dimensional FE models using ANSYS® that realistically simulate bond behavior at the epoxy-concrete interface. The outcomes of this study are expected to provide researchers, design engineers, and strengthening practitioners with valuable insights into the coupled shear-flexural response of NSM FRP-strengthened beams, as well as reliable predictive tools for avoiding debonding failures. Ultimately, this work aims to enhance the safety, efficiency, and reliability of NSM FRP retrofitting applications in civil engineering practice.

2. Experimental Program

2.1 Test specimen

To investigate their flexural-shear behavior, four RC beams measuring 2500 mm in total length and 150 x 250 mm in rectangular section were built and tested. Three beams were strengthened with NSM CFRP bars, and one beam was tested without strengthening. Two deformed steel bars with a diameter of 10 mm made up the tension and compression reinforcements. Smooth steel stirrups with a diameter of 8 mm and a regular spacing of 100 mm made

up the shear reinforcement. The tested beam's geometry and reinforcing details are displayed in Figure 1.

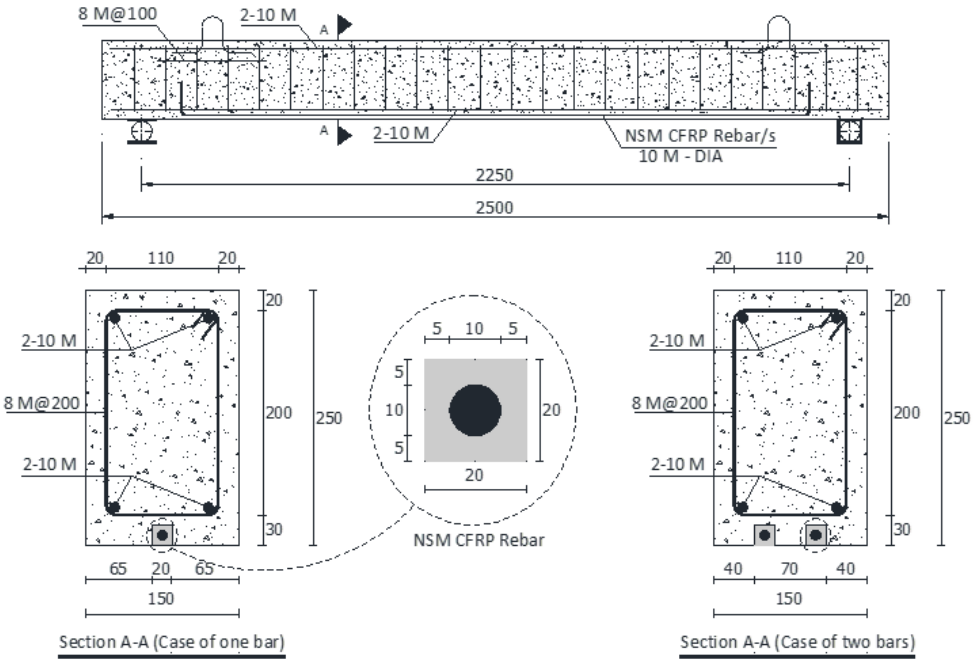

Figure 1. Details of the tested beams

2.2 Material properties

A ready-mixed concrete with a 28-day compressive strength of 28 MPa was used to cast all of the tested beams. Six conventional concrete cylinders (150 x 300 mm) were used to measure the concrete's compressive strength in accordance with ASTM C39 [15]. ASTM A370 [16] was used to determine the characteristics of the reinforcing steel. The yield and ultimate tensile strains were 0.0031 and 0.055, respectively, whereas the yield stress, ultimate strength, and modulus of elasticity were 560 MPa, 630 MPa, and 185 GPa. In this work, MBRACE-ADH 4000 (BASF) epoxy glue was utilized. The adhesive's tensile strength and modulus of elasticity are 32 and 4300 MPa, respectively, according to the manufacturer. The CFRP bars had a nominal diameter of 10 mm and a distorted surface configuration. According to ACI 440, the uniaxial tension tests yielded the tensile strength and modulus of elasticity for the utilized CFRP bars.3R-12 [17] were 130 GPa and 1800 MPa, respectively.

2.3 Specimens and Strengthening Technique

A ready-mixed concrete with a 28-day compressive strength of 28 MPa was used to cast all of the tested beams. Six conventional concrete cylinders (150 x 300 mm) were used to measure the concrete's compressive strength in accordance with ASTM C39 [15]. ASTM A370 [16] was used to determine the characteristics of the reinforcing steel. The yield and ultimate tensile strains were 0.0031 and 0.055, respectively, whereas the yield stress, ultimate strength, and modulus of elasticity were 560 MPa, 630 MPa, and 185 GPa. In this work, MBRACE-ADH 4000 (BASF) epoxy glue was utilized. The adhesive's tensile strength and modulus of elasticity are 32 and 4300 MPa, respectively, according to the manufacturer. The CFRP bars had a nominal diameter of 10 mm and a distorted surface configuration. According to ACI 440, the uniaxial tension tests yielded the tensile strength and modulus of elasticity for the utilized CFRP bars.3R-12 [17] were 130 GPa and 1800 MPa, respectively.

Horizontal and vertical foam inserts were inserted into the casting molds to pre-form square slots with a side length of 20 mm in order to place the NSM bars. The internal surfaces of the prefabricated grooves were meticulously roughened and then cleaned with pressured air prior to the NSM bars being bonded to them. In accordance with the manufacturer's instructions, the two-component epoxy was combined in a high-speed mixer. The epoxy paste was poured into each groove until it covered roughly two thirds of its volume. The bonding agent was displaced by gently pressing the CFRP bar into the groove. The groove was then fully filled with additional adhesive. After using a spatula to remove any extra epoxy, the surface was meticulously polished. Before testing, the epoxy adhesive was allowed to set for a week at room temperature.

One beam was used as a control beam for comparison and was tested without any strengthening. NSM CFRP bars with a maximum length of 2000 mm and two distinct end conditions (straight and bent) were used to reinforce three beams (S1F, S2F, and A2F). The height of the bent ends was 100 mm. One straight bar was used to reinforce Beam S1F. Two straight bars were used to reinforce Beam S2F. Two bars with bent ends were used to reinforce Beam A2F. The bent ends serve as end anchors that could postpone the CCS failure.

2.4 Test Setup and Instrumentation

The four beams underwent three-point bending tests with a concentrated load applied at the mid-span till failure and a clear flexural span of 2250 mm. A 500 kN capacity load cell was used to monitor the load, which was applied using a 1000 kN capacity servo-controlled hydraulic jack. The deflection at the midspan and beneath the loading locations was measured using three linear variable displacement transducers (LVDT) with a 120 mm range. Electrical resistance 120-ohm strain gauges were used to track strains at the level of the NSM CFRP bar and main tension steel at the midspan. Additionally, two PI gauges were fastened to one of the tested beam sides in order to measure the tensile and compressive strains in the concrete.

3. Results and discussion

The flexural behavior of the tested beams is summarized in Table 1. The final column of the table shows the failure mode of each tested beam. Below is a discussion of how the test variables affecting the tested beam's flexural response. The yielding load and its accompanying deflection are represented by Py and Δy in this table, the ultimate load and its associated deflection by Pu and Δu, the energy absorption (defined as the area under the (P-Δ) curve) by Ω, and the effective pre-yield stiffness by Ke.

TABLE 1. KEY POINTS OF LOAD-DEFLECTION CURVES; COMPARISON OF TEST RESULTS WITH FE

Beam ID	Results	P_y	Δ_y	P_u	Δ_u	K_e	Ω,	FM
		kN	mm	kN	mm	kN/m	kN.mm	
CB	Test	31.9	7.9	38.5	26.6	3112.6	2373.6	CC
	FE	29.8	7.1	38.7	22.3	3137.3	2179	CC
	Error (%)	-6.6	-10.3	0.52	-16.2	0.79	-8.2	
S1F	Test	50.3	9.7	78.8	29.3	4568.1	1905.4	CCS
	FE	48.2	9.2	84	31.9	4636	1980	CCS
	Error (%)	-4.2	- 5.5	6.5	-1.1	-0.8	3.9	
S2F	Test	72.7	10.6	102.5	20.6	6289.8	1386.1	CCS
	FE	69	9.75	106	20.4	6201.5	1311	CCS
	Error (%)	-5	-8	3.41	-1.25	1.4	-5.4	
	Test	70.5	10	108	24.9	6502.7	1787.3	CCS

A2F	FE	67.8	9.75	112	23.3	6256.5	1701	CCS
	Error (%)	- 3.87	- 2.5	3.7	- 6.6	-3.7	- 4.8	

3.1 Failure Modes and Load-Deflection Behavior

Failure modes of the strengthened beams are presented in Fig. 2. The control beam (CB) failed by concrete crushing after yielding of the steel reinforcement, while beams S1F, S2F, and A2F failed by concrete cover separation (CCS). The CCS started in beam S1F by the formation of a flexural shear crack initiated near the constant moment zone, while it started by the formation of a shear crack near the end of the CFRP bar in the two other beams.

The load-midspan deflection (P-Δ) response of the tested beams is shown in Figure 4. Generally, the beams exhibited a semi-tri-linear response defined by three stages. The first stage corresponds to the beam behaviour before cracking. The behaviour in this stage was linear elastic and the NSM reinforcement did not contribute to increase the stiffness. In the second stage, the beam started to crack at the midspan section where the maximum moment was located. Further increase of load, the cracks became wider and new flexural cracks initiated. Many uniformly distributed narrow cracks, with different depths, were observed along the whole length of the tested beam. The developed cracks did not cross the adhesive because of its low elastic modulus. Furthermore, a nonlinear behaviour was observed up to failure. In this stage, the NSM reinforcement significantly increased the stiffness, and decreased the crack widths comparing with the control beam. The second stage ends with yielding of the steel reinforcement. Comparing to the control beam (CB), the yielding load was increased by 57.70% for beam S1F, while it increased by 127.9% and 121.00% for beams S2f and A2F, respectively.

The third stage starts by yielding of the steel reinforcement and ends with the failure of the tested beams. After the steel yielding, the crack width was controlled by the NSM bar. The global stiffness of the tested beams decreased in this stage due to yielding of the steel reinforcement and the weak modulus of the NSM reinforcement. The percentage increase in strength of each beam over the control beam is illustrated in Table 1. As indicated from Table 1, using the NSM CFRP bars significantly increased the ultimate carrying capacity of the strengthened beams compared with the un-strengthened beam. Beam S1F, strengthened with one straight CFRP bar, failed at a load of 78.5 kN; achieving 104.70% increase in the ultimate load over the control beam. As the failure was governed by CCS, doubling the FRP area increased the ultimate load up to 102.50 KN for beam S2F recording 166.25% over that of control beam. The A2F beam, strengthened with two fully bonded end-anchored bars, failed at a load of 108 KN with 180.55% and 5.40% increases over the control and S2F beams, respectively. Therefore, the end hooks were effective in delaying the CCS failure and subsequently increasing the ultimate load.

3.2 Cracking Behavior of the tested beams

Generally, cracking behavior of the tested beam is divided into two phases: the crack formation phase and stabilized cracking phase. In the first phase, the cracks formed at random locations according to locally weak sections. At each cracked section, the bond action between concrete and steel was lost and the tensile stress in concrete dropped to zero. Away from the crack, the concrete was able to pick up tensile stresses until the bond action was again lost and a new crack started to from at a certain distance. This distance is identified as the crack spacing, which mainly depends on the bond properties (i.e. the better bond between concrete, steel, and NSM reinforcement, the shorter crack spacing). As the strengthened beams were tested with the same tensile steel area, the crack spacing differed from a beam to another according to the bond between concrete and NSM reinforcement.

Doubling the FRP cross sectional area in beam S2F reduced the crack spacing compared to beam S1F; this is because increasing the FRP area decreased the developed tensile force in the CFRP bar, which enhanced the bond between concrete and NSM reinforcement.

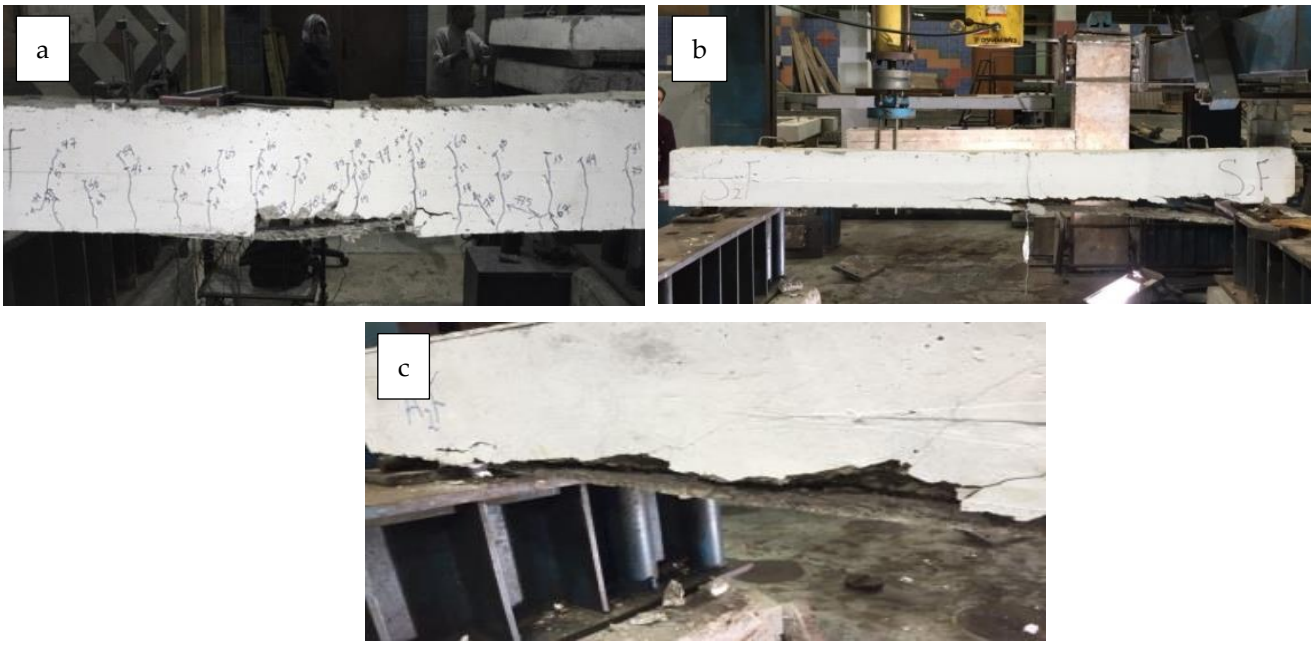

Figure 2. Failure modes of the tested beams (a) Beam S1F, (b) Beam S2F and (c) Beam A2F

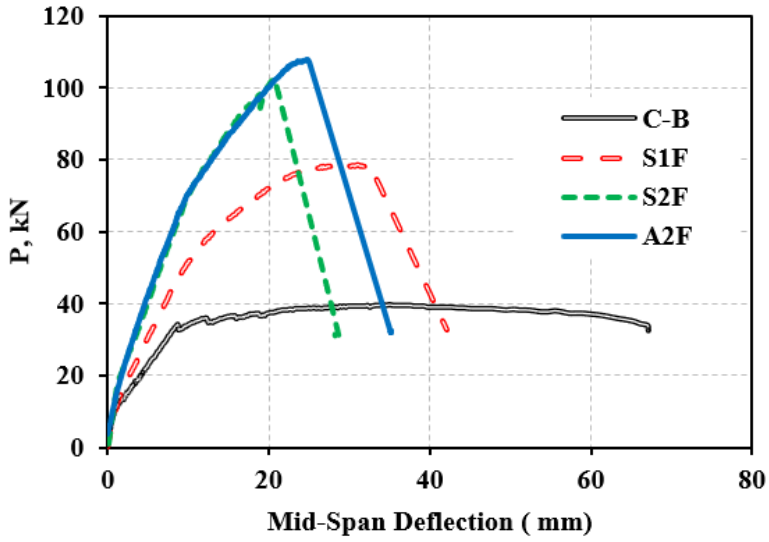

Figure 3. Load-deflection curves for the tested beams

3.3 Load-Strain Response at the Midspan of the Tested Beams

In this section, the load-strain (P-ε) response is discussed and compared for the tested beams. The (P-ε) responses in the CFRP bar, tension steel and extreme compression fiber of concrete at the midspan location are shown in Fig. 4.

Generally, up to concrete cracking in tension, the strain increased in a linear manner with the increase of the applied load. After cracking, all the tensile forces carried by concrete were transferred to the tension steel and NSM reinforcement. As a result, the flexural stiffness of the beam decreased causing a reduction in the slope of the (P-ε) curve; however, the

relation remained linear up to yielding of the tension steel. After yielding, the flexural stiffness of the beam was significantly reduced and another decrease occurred in the slope of the (P-ε) curves.

Response was similar to the load-deflection (P-Δ) response. Strengthening with two CFRP bars instead of one bar in beam S2F significantly decreased the developed CFRP strains at the same load compared with beam S1F. Existence of the end anchors in beam A2F reduced the developed CFRP strains compared to beam S2F. The CFRP bars reached 8702 με and 5719 με at the failure of beams S1F and S2F, respectively. Therefore, with respect to beam S1F, doubling the cross-sectional area of the CFRP bars reduced the developed FRP strain at failure by 34.3%. Doubling the NSM CFRP shifted the initiation point of the CCS failure. The CFRP bars reached 6611 με at the failure of beam A2F achieving a 15.5% increase over beam S2F.

The measured steel strain at yielding ranged between 2932 με and 3731 με, which is slightly higher than the average yield strain of 3111 με for the tested steel bars. This is possibly due to the tension stiffening effect generated at the bottom of the tested beams. It can be seen in Fig. 4 that doubling the cross-sectional area of the CFRP bars in beam S2F significantly decreased the measured steel strains at the same load levels compared to beam S1F. Strains in the top compression fibers of concrete were calculated based on the linear extension of the recorded strain readings which were measured using the PI-displacement transducers.

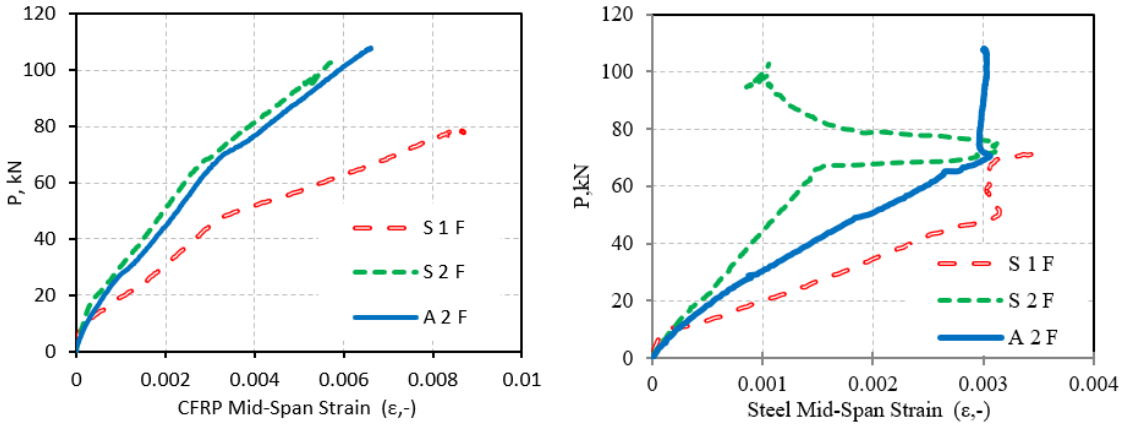

(a) (b)

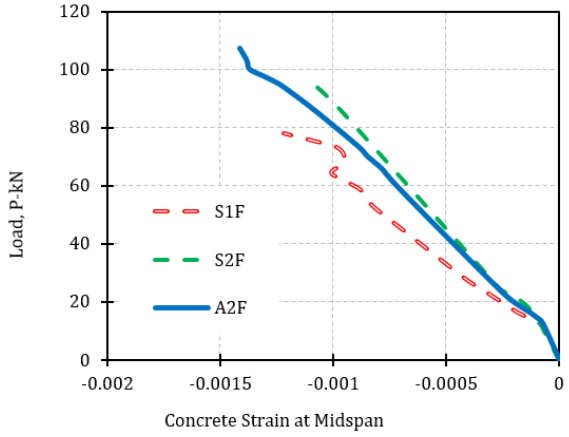

(c)

Figure 4. Load-midspan strain responses of the tested beams (a) Load-CFRP strain response, (b) Load-steel strain response and (c) Load-concrete strain response

3.4 Finite Element Model

Only one quarter of the RC beam was modelled due to the symmetry of geometry and loading conditions. A double symmetry case was simulated by restraining the displacements in the directions perpendicular to the symmetry planes.

Eight-node solid brick element (SOLID65) was used to model the concrete and epoxy adhesive. The crushing capability of the solid element was removed for concrete to prevent the premature local failure due to stress concentration under loading plates. The steel reinforcement and NSM CFRP bars were modelled using 3D 2-Node structural bar element (LINK180). The perfect bond (No slip occurrence) was considered between the steel reinforcement and concrete as well as between the NSM bar and epoxy. Eight-node solid brick element (SOLID185) was used to model the loading and supporting apparatus. The element is defined by eight nodes having three degrees of freedom at each node, translations in nodal x, y, and z, with the capability of considering nonlinearity and large deformations.

A multi-linear plastic damage model along with the William and Warnke model were employed to define the failure of concrete. The non-linear plastic behavior of concrete under uniaxial compression was obtained from the Hognestad model. The tensile stress-strain response of concrete is shown in Figure 5

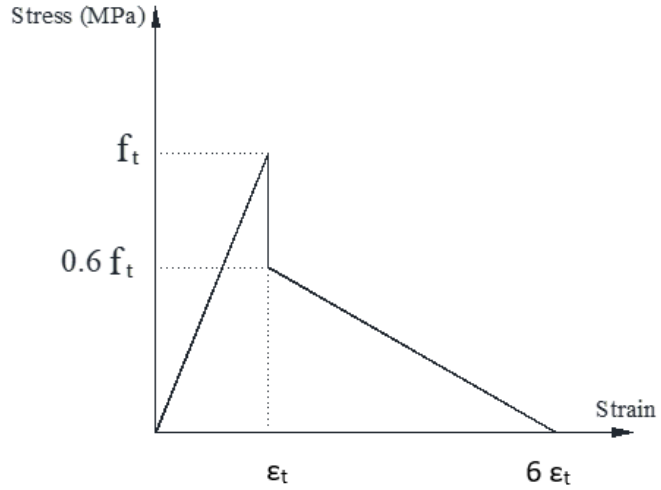

Figure 5. Constitutive model of concrete in tension

The steel reinforcement was assumed to have an elastic-perfectly plastic response with a poison's ratio of 0.30. The Von-Misses failure criterion was used to define yielding of the steel reinforcement. The steel loading and supporting apparatus were modelled as rigid elastic material with a modulus of elasticity and poison's ratio of 200 GPa and 0.30, respectively. The CFRP material was considered to be linear elastic up to failure. A multi-linear elasto-plastic diagram was used to define the adhesive behaviour along with the same concrete cracking model, but without considering the tension softening phenomenon. A Poison's ratio of 0.35 and 0.37 was assumed for the CFRP and epoxy adhesive, respectively.

3.5 Epoxy-Concrete Interaction

Debonding at the epoxy-concrete interface is analyzed by using cohesive zone material (CZM) model and fracture mechanics. Both, contact and interface elements, with zero and finite thickness, respectively, can use the CZM traction-separation constitutive model in ANSYS®. The contact elements were used for the FE models of the non-anchored NSM systems (in S1F and S2F beams), while the interface elements were used for the FE models of the anchored NSM systems (in the A2F beam). A mixed-mode bilinear CZM model, predefined in

ANSYS®, was used to simulate the interface debonding. In such a model, the interface separation occurs under a combination of three traction modes (mode I: opening, mode II: shear, and mode III: tearing); therefore, this type of debonding is controlled by both shear-slip (Γ-δ) and tension-gap (6-u) behaviours. The bilinear shear-slip and tension-gap behaviours are presented in Fig.6.

The ultimate tensile stress (6max) and tensile fracture energy (Gcn) were limited to the tensile strength (ft) and fracture energy of concrete (Gft). The tensile fracture energy of concrete was using Eq. 1, which is proposed by CEB-FIP model code. The contact gap at completion of debonding (uf) was obtained using Eq. 2, which was derived by equating the tensile fracture energy of the interface with the tensile fracture energy of concrete. To obtain the maximum interfacial shear stress (Γmax), Eq. 3 which was proposed by Hassan and Rizkalla was used. An extensive parametric study was conducted to determine the contact slip at completion of debonding (δf). The value of δf was taken as 0.35 and 0.25 for beams strengthened with one and two CFRP bars, respectively. The separations values (uu and δu) were assumed to be one quarter of the failure separation values (uf and δf).

$$G_{ft} = (0.0469\ Da^2 - 0.5\ Da + 26)\left(\frac{f'c}{10}\right)^{0.70} \quad \text{Eq. 1}$$

$$u_f = \frac{f_c'^{0.2}}{1.40}(0.0469\ D_a^2 - 0.5\ D_a + 26) \quad \text{Eq. 2}$$

$$\Gamma_{max\ (epoxy\text{-}concrete)} = \frac{fi\ \mu}{1.40} \quad \text{Eq. 3}$$

Where Da is the maximum aggregate size and μ is the epoxy-concrete friction coefficient; a value of μ = 1 was used [2].

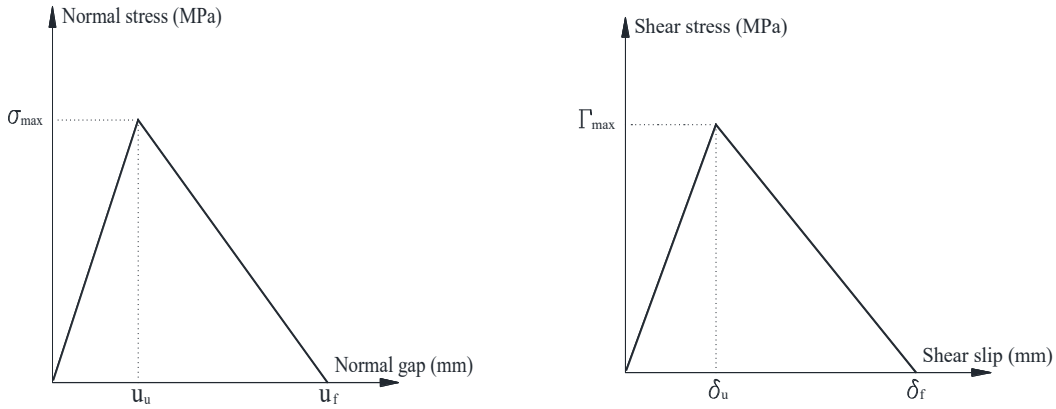

(a) (b)

Figure 6. Bilinear Normal-gap and shear-slip models, (a) Normal-gap model and (b) Shear-slip model

3.6 Non-Linear Analysis

The non-linear solution was operated using a force control mode with a 10 N load increment. In contrast with the displacement control mode, the force control mode consumes a little time in solving such complex models; however, it cannot track the post-peak behaviour of the modelled specimen. The FE models were developed with refined mesh applied at the locally high stressed zones. Fig. 7 shows the used mesh in the developed models.

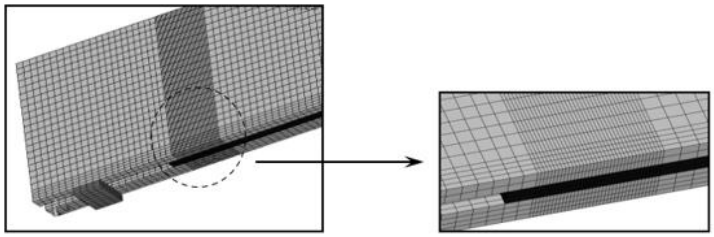

Figure 7. Mesh of the developed FE models

Failure of the developed FE models was defined according to two mechanisms: (a) crushing of the concrete after yielding of the steel reinforcement and (b) concrete cover separation. The modelled specimen is considered to be failed by concrete crushing if the compressive strain reaches the value of 0.003. The concrete cover separation was detected by the examination of the equivalent plastic strain of concrete at the level of the failure plane which was experimentally observed. The modelled RC beam was assumed to fail by CCS when the effective plastic tensile strain at the level of the tension steel exceeds the rapture strain of concrete.

3.7 Finite Element Results

3.7.1 Validation of the FE results

Fig. 8 shows a comparison between the experimental and numerical load-deflection curves for all the tested RC beams. At yielding stage, the differences between the experimental and FE values are negligible. However, the obtained ultimate loads from the FE models are slightly higher than those obtained from the experimental records. This in fact is due to ignoring the radial stresses transferred from the tension steel and NSM bars to the concrete in the developed FE models. The comparison details are enlisted in Table 1.

The comparison indicates that there is a good correlation between the developed models and the recorded experimental results at all stages of loading up to failure. The FE load-CFRP strain response at the midspan was compared to that obtained from the experimental results in Fig. 9. Generally, the slight differences between the analytical and experimental results can be related to the CFRP modulus, which is not absolutely constant and could be slightly smaller or greater than the specified value. Based on the compared load-deflection behaviour, load-CFRP strain response, and failure modes, both validity of the developed FE models and reliability of the FE simulation are confirmed.

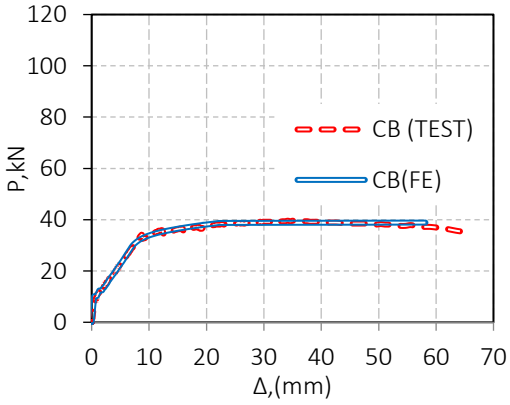

(a)

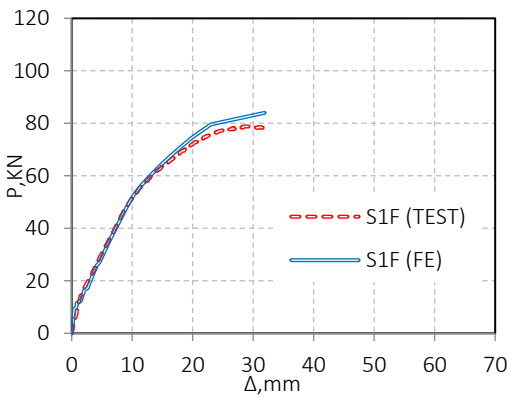

(b)

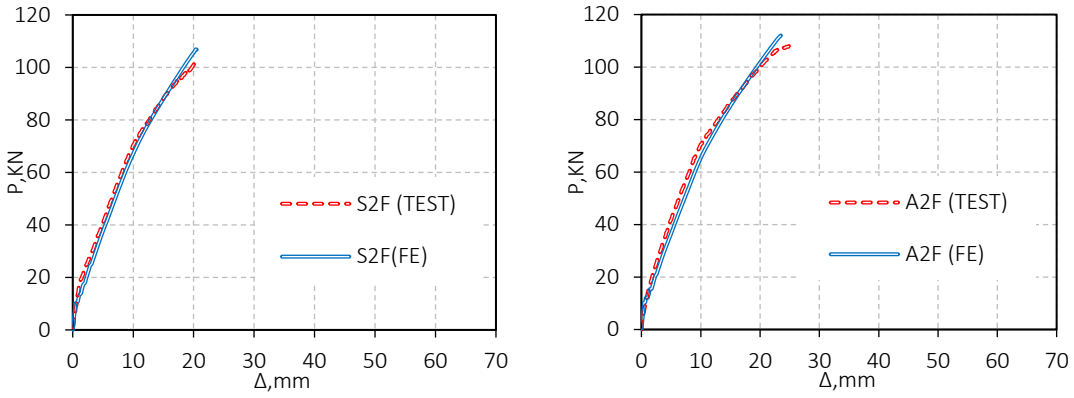

(c) (d)

Figure 7. Comparison between the obtained experimental and numerical (P-Δ) curves

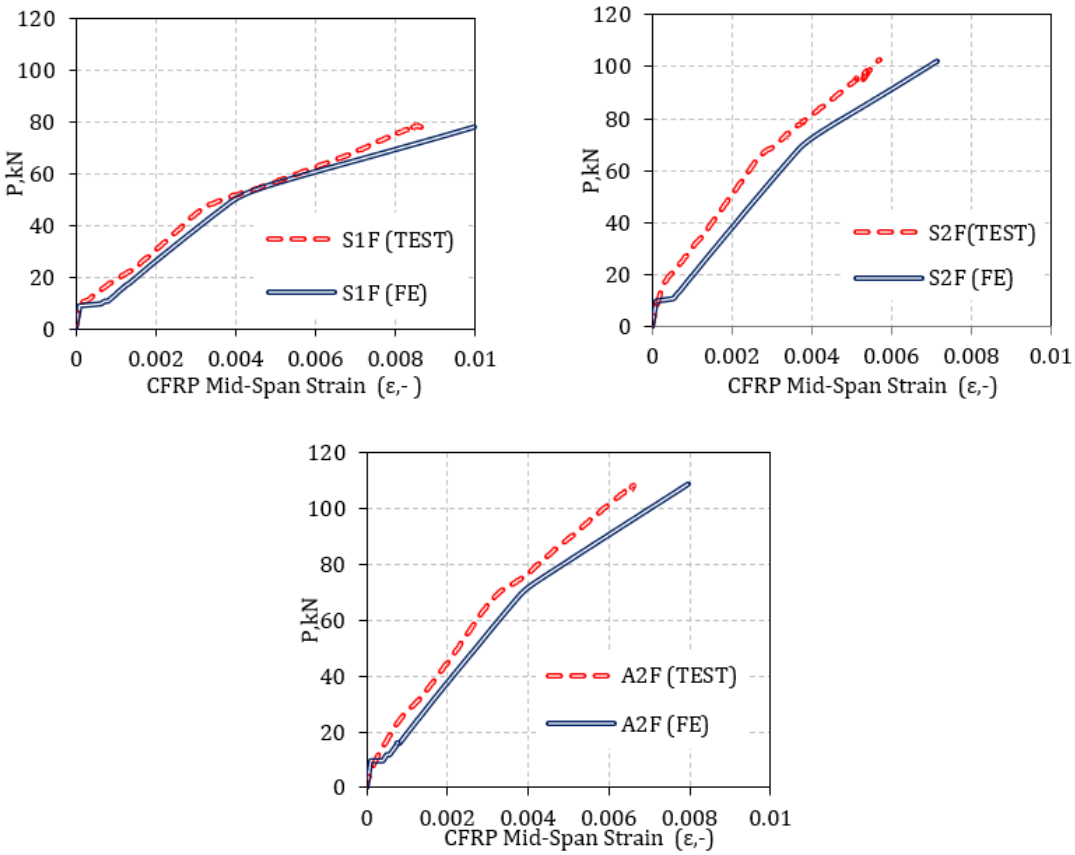

Figure 7. Comparison between the experimental and numerical load-CFRP strain curves

4. Conclusions

The following key conclusion can be made in light of the given experimental and numerical results:

1. Flexural strength and stiffness can be greatly increased by strengthening with NSM CFRP bars. The NSM strengthening system reduced the deflections and crack widths at various loading stages and enhanced the tested beams' load-deflection response. The most common mode of failure for all the strengthened beams was the separation of the concrete cover.

2. Compared to a beam strengthened by a single straight bar, it is evident that doubling the FRP cross area results in a very large improvement in the final carrying capacity and stiffness, scoring 29.6% and 37.7%, respectively.
3. Compared to straight CFRP bars, strengthening using end-anchored CFRP bars enhanced the ultimate load and postponed the CCS failure.
4. The flexural behavior of RC beams reinforced with NSM anchored and non-anchored CFRP bars was accurately reproduced by the established FE models. The established FE models' cracking behavior might be replicated by the strain-based failure criteria utilized to predict the CCS failure mode.

Author Contributions: For this research articles with one author, "Conceptualization, Abd Al-Kader A. Al Sayed and A. Ali; methodology, Abd Al-Kader A. Al Sayed.; software, Amr Abdelkhalik and A. Ali.; validation, Abd Al-Kader A. Al Sayed.; formal analysis, Amr Abdelkhalik.; investigation, Abd Al-Kader A. Al Sayed.; resources, Amr Abdelkhalik.; data curation, Amr Abdelkhalik.; writing—original draft preparation, Abd Al-Kader A. Al Sayed and A. Ali.; writing—review and editing, Amr Abdelkhalik.; visualization, Abd Al-Kader A. Al Sayed.; supervision, Amr Abdelkhalik.; project administration, Abd Al-Kader A. Al Sayed.; funding acquisition, Abd Al-Kader A. Al Sayed. Author has read and agreed to the published version of the manuscript."

Funding: This research received no external funding

Data Availability Statement: Data Availability Statement: The original contributions presented in this study are included in the article. Further inquiries can be directed to the corresponding author.

Conflicts of Interest: The authors declare no conflicts of interest.

References

[1] S. S. Zhang, Y. Ke, E. Chen, H. Biscaia, and W. G. Li, "Effect of load distribution on the behaviour of RC beams strengthened in flexure with near-surface mounted (NSM) FRP," *Compos. Struct.*, vol. 279, no. September 2021, 2022, doi: 10.1016/j.compstruct.2021.114782.

[2] S. S. Mohamed, O. Hamdy, M. H. Seleem, and I. A. Sharaky, "The flexural behavior and efficiency of RC beams strengthened with SNSM bars under the effect of several end conditions and material properties," *Eng. Struct.*, vol. 308, no. April, p. 117990, 2024, doi: 10.1016/j.engstruct.2024.117990.

[3] Y. J. Kim, S. W. Hyun, J.-Y. Kang, and J.-S. Park, "Anchorage configuration for post-tensioned NSM CFRP upgrading constructed bridge girders," *Eng. Struct.*, vol. 79, pp. 256–266, 2014, doi: https://doi.org/10.1016/j.engstruct.2014.08.022.

[4] W. Ge, W. Song, A. F. Ashour, W. Lu, and D. Cao, "Flexural performance of FRP / steel hybrid reinforced engineered cementitious composite beams," *J. Build. Eng.*, vol. 31, no. December 2019, p. 101329, 2020, doi: 10.1016/j.jobe.2020.101329.

[5] A. El Refai, F. Abed, and A. Al-Rahmani, "Structural performance and serviceability of concrete beams reinforced with hybrid (GFRP and steel) bars," *Constr. Build. Mater.*, vol. 96, pp. 518–529, 2015, doi: 10.1016/j.conbuildmat.2015.08.063.

[6] W. Gang, W. Zhi-Shen, L. Yun-Biao, S. Ze-Yang, and H. Xian-Qi, "Mechanical Properties of Steel-FRP Composite Bar under Uniaxial and Cyclic Tensile Loads," *J. Mater. Civ. Eng.*, vol. 22, no. 10, pp. 1056–1066, Oct. 2010, doi: 10.1061/(ASCE)MT.1943-5533.0000110.

[7] S. Moolaei, M. K. Sharbatdar, and A. Kheyroddin, "Experimental evaluation of fl exural behavior of HPFRCC beams reinforced with hybrid steel and GFRP bars," *Compos. Struct.*, vol. 275, no. February, p. 114503, 2021, doi: 10.1016/j.compstruct.2021.114503.

[8] A. Palmieri, S. Matthys, and L. Taerwe, "Experimental investigation on fire endurance of insulated concrete beams strengthened with near surface mounted FRP bar reinforcement," *Compos. Part B Eng.*, vol. 43, no. 3, pp. 885–895, 2012, doi: https://doi.org/10.1016/j.compositesb.2011.11.061.

[9] T. Abdelaleem and H. M. A. Diab, "Suggestions for repairing various defects in the NSM strengthening mechanism with hybrid rebars for RC beams: Experimental and numerical study," *Eng. Struct.*, vol. 289, p. 116225, 2023, doi: https://doi.org/10.1016/j.engstruct.2023.116225.

[10] X. Li, G. Xing, Z. Chang, and J. Huang, "Experimental and analytical study of RC beams strengthened with prestressed near-surface mounted 7075 aluminum alloy bars," *Structures*, vol. 48, pp. 1693–1706, 2023, doi: https://doi.org/10.1016/j.istruc.2023.01.065.

[11] I. A. Sharaky, S. A. I. Selmy, M. M. El-Attar, and H. E. M. Sallam, "The influence of interaction between NSM and internal reinforcements on the structural behavior of upgrading RC beams," *Compos. Struct.*, vol. 234, no. October 2019, p. 111751, 2020, doi: 10.1016/j.compstruct.2019.111751.

[12] R. H. Haddad and Y. T. Obaidat, "A nonlinear finite element model for shear deficient heat-damaged concrete beams repaired using NSM CFRP strips," *Constr. Build. Mater.*, vol. 170, pp. 314–325, 2018, doi: https://doi.org/10.1016/j.conbuildmat.2018.03.084.

[13] J. Hwang, D. Seo, K. Park, and Y. You, "Experimental Study on the Mechanical Properties of FRP Bars by Hybridizing with Steel Wires," no. June, pp. 365–373, 2014.

[14] M. M. Attia, A. A. El-Latief, and M. A. Eita, "Performance of RC beams with novelty GFRP under the bending load: An experimental and FE study," *Case Stud. Constr. Mater.*, vol. 18, no. February, p. e02000, 2023, doi: 10.1016/j.cscm.2023.e02000.

[15] Z. Cai, W. Yuan, Z. Wang, and S. T. Smith, "Seismic behavior of precast segmental bridge columns reinforced with hybrid FRP-steel bars," *Eng. Struct.*, vol. 228, no. October 2020, p. 111484, 2021, doi: 10.1016/j.engstruct.2020.111484.

[16] U. Ebead and H. El-Sherif, "Near surface embedded-FRCM for flexural strengthening of reinforced concrete beams," *Constr. Build. Mater.*, vol. 204, pp. 166–176, 2019, doi: https://doi.org/10.1016/j.conbuildmat.2019.01.145.

[17] H. Y. Leung, "Flexural behaviour of concrete beams internally reinforced with GFRP rods and steel rebars," vol. 21, no. 4, pp. 146–157, 2003, doi: 10.1108/02630800310507159.

[18] D. Zhou, Y. Mei, X. Ke, Z. Liu, and W. Xu, "Study on the structural behavior and reinforcement design of openings in subway station floor slabs," *J. Build. Eng.*, vol. 98, p. 110994, 2024, doi: https://doi.org/10.1016/j.jobe.2024.110994.

[19] M. Adem Yimer and T. Dey, "Dynamic response of concrete beams reinforced with GFRP and steel bars under impact loading," *Eng. Fail. Anal.*, vol. 161, p. 108329, 2024, doi: https://doi.org/10.1016/j.engfailanal.2024.108329.

[20] O. Elharouney, M. Elkateb, and A. Khalil, "Behaviour of prestressed hollow core slabs strengthened with NSM CFRP strips around openings: A finite element investigation," *Eng. Struct.*, vol. 238, p. 112262, 2021, doi: https://doi.org/10.1016/j.engstruct.2021.112262.

[21] D. Alwash, R. Kalfat, and R. Al-Mahaidi, "Numerical modelling of RC beams strengthened in shear using NSM FRP and cement based adhesives," *Structures*, vol. 57, p. 105217, 2023, doi: https://doi.org/10.1016/j.istruc.2023.105217.

[22] Z. Sun *et al.*, "Experimental study on the fl exural behavior of concrete beams reinforced with bundled hybrid steel / FRP bars," *Eng. Struct.*, vol. 197, no. July, p. 109443, 2019, doi: 10.1016/j.engstruct.2019.109443.

[23] A. A. Shukri, M. A. Hosen, R. Muhamad, and M. Z. Jumaat, "Behaviour of precracked RC beams strengthened using the side-NSM technique," *Constr. Build. Mater.*, vol. 123, pp. 617–626, 2016, doi: https://doi.org/10.1016/j.conbuildmat.2016.07.066.

[24] S. Ahmed, I. A. Sharaky, Y. E. Ibrahim, and A. Abdo, "Flexural response of GFRP RC beams strengthened with side and bottom NSM GFRP bars," *Case Stud. Constr. Mater.*, vol. 18, p. e01858, 2023, doi: https://doi.org/10.1016/j.cscm.2023.e01858.

[25] H. Song, Q. Chun, Y. Han, X. Gao, and Z. Cui, "Research on flexural behavior of square and circular cross-section timber beams strengthened with externally bonded and near-surface-mounted hybrid FRP plates," *Constr. Build. Mater.*, vol. 451, p. 138742, 2024, doi: https://doi.org/10.1016/j.conbuildmat.2024.138742.